Applied Catalysis B: Environmental 236 (2018) 13–24

Contents lists available at ScienceDirect

Applied Catalysis B: Environmental

journal homepage: www.elsevier.com/locate/apcatb

Catalytic co-aromatization of methane and heptane as an alkane model compound over Zn-Ga/ZSM-5: A mechanistic study

Qingyin Li[a], Peng He[a], Jack Jarvis[a], Amit Bhattacharya[b], Xiaohui Mao[c], Aiguo Wang[a], Guy M. Bernard[b], Vladimir K. Michaelis[b], Hongbo Zeng[c], Lijia Liu[d], Hua Song[a,*]

[a] Department of Chemical and Petroleum Engineering, University of Calgary, 2500 University Drive NW, Calgary, Alberta T2N 1N4, Canada
[b] Department of Chemistry, University of Alberta, 11227 Saskatchewan Drive, Edmonton, Alberta T6G 2G2, Canada
[c] Department of Chemical and Materials Engineering, University of Alberta, 9211-116 Street NW, Edmonton, Alberta T6G 1H9, Canada
[d] Jiangsu Key Laboratory for Carbon-Based Functional Materials & Devices, Institute of Functional Nano and Soft Materials (FUNSOM), Soochow University-Western University Centre for Synchrotron Radiation Research, Soochow University, Suzhou, Jiangsu 215123, China

ARTICLE INFO

Keywords:
Aromatization
Methane-^{13}C
Methane activation
ZSM-5
Catalyst

ABSTRACT

The joint conversion of methane and heptane, a model compound of paraffin-rich raffinate oil, over a Zn-Ga modified zeolite catalyst has been investigated at various reaction times. In comparison with the performance from a N_2 environment, the introduction of methane highly promotes the formation of light aromatic compounds with a single phenyl ring, and increased carbon number and substitution index of chemical constituents formed are indicative of methane incorporation into the liquid product. In addition, with prolonged time, the interaction between catalyst and methane molecules is enhanced. Through cleavage of methane molecules, the formed moieties likely participate in the aromatization reaction, which results in the growth of larger aromatic components through further condensation. According to the NMR spectra, witnessing methane engagement into the phenyl carbon and alkyl carbon sites of the formed liquid aromatics along with increasing reaction time is evidenced ^{13}C-methane incorporation into aromatics. The excellent catalytic performance of Zn-Ga/ZSM-5 might be ascribed to the greatly dispersed metal species on the catalyst surface as well as a certain amount of medium and weak acid sites. With regards to the spent catalyst, the presence of methane could inhibit the aggregation of loaded active metals and coke formation during the co-aromatization process. The elucidation on the co-conversion of methane and high alkane provides great potential for the utilization of natural gas resources and intermediates formed from petrochemical industries.

1. Introduction

With the recently increasing demands for new energy sources due to the depletion of petroleum resources and global environmental concerns, methane, being the dominant component in natural gas, methane hydrate and shale gas, is considered as a potential alternative hydrocarbon feedstock for the synthesis of valuable petrochemicals [1–3]. However, although these methane-containing resources play a key role in meeting the requirement of human society's needs, it is well known that methane is the least reactive hydrocarbon molecule due to its strong C—H bond energy of 435 kJ/mol [4,5]. Thus, major efforts are required for its activation and conversion into higher hydrocarbons, which limits its commercial application to a large extent. Currently, conventional methane utilization depends greatly on the multi-step syngas strategy, which incurs large energy consumption and lacks product selectivity [6]. Therefore, many contributions have been made to direct methane conversion under mild conditions with the application of suitable catalysts [7,8].

Due to thermodynamic limitations, the oxidative coupling of methane to produce valuable chemicals such as ethane and ethylene have been impeded even with various catalytic systems employed, which highly restricts its industrial application [9]. On the other hand, attention has also been focused on the non-oxidative activation of methane to obtain high value-added chemicals such as aromatics, which have been investigated extensively over the past few decades [10–12]. However, the majority of the reports on direct methane conversion into aromatic compounds in the literature is implemented at extremely high temperatures (> 1000 K). Choudhary et al. pioneered the co-conversion of methane and alkanes over transition metal modified catalysts to produce higher hydrocarbons [13,14]. It seems that hydrocarbon-involved methane aromatization can overcome the thermodynamic limitation associated with the conversion of methane alone, and thus the

* Corresponding author.
E-mail address: sonh@ucalgary.ca (H. Song).

https://doi.org/10.1016/j.apcatb.2018.05.006
Received 31 December 2017; Received in revised form 4 April 2018; Accepted 3 May 2018
Available online 04 May 2018
0926-3373/

presence of a co-reactant makes methane activation feasible under mild conditions. Some investigations on the co-aromatization of methane and hydrocarbons, such as ethane, propane, pentane and light gasoline, over various types of zeolite catalysts have been previously reported [15–18]. Gim et al. [19] have exemplified the excellent catalytic performance of GaO_y supported on mesoporous HZSM-5 for the co-aromatization of methane and propane for benzene, toluene, xylene (BTX) production due to enhanced mass transfer and acidity. He et al. [20] investigated the simultaneous aromatization of propylene and methane over a Ag-Ga loaded HZSM-5 catalyst, and the increased average carbon number of the formed products was attributed to methane incorporation into the aromatics. Anunziata et al. [21] observed the significant promotion of methane activation using hexane as a co-reactant over Zn/HZSM-11 zeolite, resulting in high conversion and aromatic yields.

As the engagement of higher hydrocarbons as co-reactants is the key point for methane activation, it is essential to understand how the synergetic mechanism unfolds during co-aromatization reactions over metal-promoted zeolite catalyst. Many researchers have tried to elucidate the reaction mechanism for the incorporation of methane into aromatic products. Isotope tracing experiments with the employment of ^{13} C-labeled methane have been conducted to detect the formed reaction intermediates on the catalyst surface via solid-state nuclear magnetic resonance (NMR) spectroscopy, which in turn provide valuable clues for reaction pathway identification during the co-aromatization of methane and higher hydrocarbons [22–24].

Based on the previous explorations concerning the conversion of biomass and heavy oil as well as cracked distillates under a methane environment, Zn and Ga-modified catalysts exhibit excellent performance on the co-aromatization reaction [25–27]. In addition, the co-aromatization of light hydrocarbons including hexane, heptane and octane under a methane environment, investigated in previous work, demonstrated that the influence of the introduced methane on heptane aromatization was more significant than that of other feedstocks. Therefore, in this paper, the feasibility of heptane co-aromatization under a methane environment over Zn-Ga/ZSM-5 is discussed comprehensively. The compositional distributions as well as carbon number and substitution degree of the formed liquid products at different reaction times are acquired to gain a better understanding of the methane effect on the liquid products. As well as this, ^{13}C-methane is introduced to confirm methane incorporation into the formed liquid products, which can provide insight into the reaction pathway during the co-aromatization reaction. The correlation between catalyst properties and its corresponding aromatization performance is explored by versatile characterization techniques.

2. Experimental

2.1. Catalyst preparation

Ammonium ZSM-5 zeolite with a SiO_2/Al_2O_3 molar ratio of 80 was supplied by *Zeolyst*. The NH_4-form powder was converted into its protonic form via calcination at 600 °C for 5 h. The Zn and Ga metal introduction into the zeolite support was achieved through conventional incipient wetness impregnation to obtain 5% zinc and 1% gallium metal loading. $Zn(NO_3)_2{\cdot}6H_2O$ (99.0%) and $Ga(NO_3)_3{\cdot}xH_2O$ (99.9%), used as the metal precursors, were purchased from Alfa Aesar. A certain amount of the metal nitrates was first dissolved in deionized water, and then the formed aqueous solution was introduced drop wise to the HZSM-5 support. Subsequently, the powder was mixed well using a mortar and pestle after drying at 90 °C overnight, and then calcined in air at 600 °C for 3 h to acquire the metal-modified catalysts.

2.2. Catalytic activity measurement

The catalytic performance was assessed using a 100-mL Parr© batch reactor. In a typical run, 0.5 g of catalyst was placed into the batch reactor uniformly covering its bottom, and the glass vial loaded with 1 g of heptane (Sigma Aldrich, 99%) was put on the catalyst layer. Once the reactor was properly sealed and passed the leak test, it was pressurized up to 30 bar using reactive gas including CH_4 or N_2 after the air inside was completely purged out. The temperature was then raised to 400 °C at a heating rate of ~20 °C/min, and maintained for the desired reaction time. When the experiment was completed, the reactor was taken out of the furnace and then immediately submerged into a water bath to quench the reaction. After the equipment was cooled down to room temperature, the remaining gases were collected for compositional analysis. The resulting liquid product was collected by extraction using 10 g CS_2, and through filtration the solid catalyst was separated from the mixture. A methane-alone experiment was also performed, without addition of heptane, as a blank run to evaluate the catalytic methane aromatization activity in the absence of a higher alkane; no detectable methane conversion nor aromatic products were observed, as expected.

In the case of the isotopic labeling reactions, the experiments were conducted using the aforementioned batch reactor. The same amount of catalyst and feedstock were charged into the reactor at 30 bar including 25 bar non-labeled methane and 5 bar $^{13}CH_4$ (99.9% ^{13}C, Cambridge Isotope Laboratories Inc.) in the gas phase. The same technique mentioned above was performed to collect the liquid product from the ^{13}C-labeled methane run. With regards to the solid sample after reaction, the spent catalyst was directly collected without CS_2 extraction for further analysis using solid-state NMR.

2.3. Catalyst characterization

The acid strength and amount of these catalysts were determined through the temperature-programmed desorption of ammonia (NH_3-TPD) performed on a Finesorb-3010 Chemisorption Analyzer equipped with a thermal conductive detector (TCD). The tested samples (approximately 0.2 g) were first activated by heating to 600 °C for 30 min under a helium flow to remove any impurities adsorbed during storage, and then cooled down to 100 °C. Subsequently, ammonia saturation of the activated catalyst was achieved by introducing a 0.5% NH_3/N_2 stream with a flow rate of 30 sccm to the packed catalyst bed. After the removal of physically adsorbed NH_3 molecules with He purging for 60 min, the samples were heated up to 600 °C at a heating rate of 10 °C/min and maintained for 60 min. The amount of released NH_3 due to heating desorption was determined by the TCD. To measure the acidity amount and its strength from ammonia desorption profiles, the curve areas were integrated by employing a Gaussian deconvolution of peaks, and the acidity amounts were expressed in terms of micromoles of ammonia per gram of catalysts.

XAS (X-ray absorption spectroscopy) measurements were carried out at the high resolution spherical grating monochromator (SGM) 11ID-1 beamline (240–2000 eV) from the Canadian Light Source synchrotron facility at the University of Saskatchewan in Saskatoon. The samples were prepared by covering carbon tape homogeneously with dispersed catalyst powder. The total electron yield (TEY) and fluorescence yield (FLY) were measured in tandem at the specific adsorption edge. For each scan, averages of 50–60 scans were taken at a new spot on each sample. The data were recorded at the Zn L edge in fluorescence mode. The spectra normalization was conducted using the incoming synchrotron beam flux (I_0) signal.

TEM (Transmission Electron Microscope) images of these catalysts were collected using a transmission electron microscope (JEOL 2100FS) operated at 200 kV. An electron energy loss spectrometer (EELS) was coupled with the equipment to determine the distribution of different elements in individual particles. Both bright-field and high-angle annual dark-field were performed to acquire the TEM images. Generally, on the basis of specific energy loss of transmitted electrons due to the ionization of inner-shell electrons, the resulting ionization edges can be employed to detect the existence of elements in the specimen. As for Zn

and Ga modified catalysts, the Zn L-shell and Ga M-shell ionization edges were utilized to map the elemental dispersion on the particular area.

XPS (X-ray photoelectron spectroscopy) were performed at nanoFAB using a Kratos Axis spectrometer with monochromatized Al Kα ($h\upsilon$ = 1486.71 eV) with a base pressure of ~5×10^{-10} Torr in the analysis chamber. The preliminary calibration of the binding energy scale was conducted through the peak position of Au $4f_{7/2}$ (binding energy = 84.0 eV) with reference to the Fermi level. The elemental binding energies were referenced to the C 1s of 284.8 eV corresponding to surface hydrocarbon-like deposits, and the inelastic background of core-level peaks was subtracted with the Shirley background employed. The core-level spectra were recorded at a pass energy of 20 eV while that for the survey spectrum collection within a range of binding energies from 0 to 1100 eV was 160 eV. Fitting of the XPS spectra was completed using the XPSPEAK (v. 4.1) program.

The ^{13}C liquid NMR (nuclear magnetic resonance) spectra were recorded at 9.4 T (ν_0 (^{13}C) = 100.6 MHz) on a Bruker Avance III 400 NMR spectrometer with a BBFQ probe. The $CDCl_3$ peak appearing at 77.23 ppm was used as a reference for the ^{13}C NMR spectra. 1000 scans were collected for each spectrum with a spectral width of 26 kHz. The recycle delays for liquid NMR were not optimized and set to 2 s. These values are probably less than the full relaxation time of carbon-13 nuclei, although employed to maximize the number of scans in each measurement and achieve a better signal to noise ratio of the spectra for direct comparison of labeled and non-labeled $^{13}CH_4$. As a result, the peak area may not be linearly proportional to the concentration of ^{13}C in the products.

Qualitative ^{13}C cross-polarization (CP) magic-angle spinning (MAS) NMR experiments for the collected catalyst samples were recorded at 7.05 T (ν_0 (^{13}C) = 75.533 MHz) on a Bruker Avance 300 NMR spectrometer. Samples were packed into 4 mm OD zirconia rotors and spun at a frequency of 12 kHz. ^{13}C data were referenced with respect to tetramethylsilane (TMS) by setting the high frequency ^{13}C peak of adamantane to 38.56 ppm. The following conditions were used for recording the spectra: the π/2 pulse was 4 μs, the contact time was 3 ms, a 3 s recycle delay (optimized from ^{1}H) and between 28k and 32k co-added transients.

2.4. Product analysis

Gas chromatography (PerkinElmer GC Claus 680) coupled with a mass spectrometer (MS Clarus SQ 8T) equipped with a Paraffins-Olefins-Naphthenes-Aromatics (PONA) column (Agilent HP-PONA) was used for the compositional analysis of the liquid products. The column temperature was initially programmed to 35 °C and maintained for 15 min, and then increased to 70 °C at the heating rate of 1.5 °C/min, and ramped up to 150 °C at 3 °C/min and held for 30 min, and finally elevated to 250 °C and held for 30 min. The molecular structure of each component in the formed liquid product was confirmed via the National institute of Standards and Technology (NIST) library.

The gas products were analyzed by a four-channel micro-GC (490, Agilent) equipped with four thermal conductivity detectors, which can precisely analyze H_2, O_2, N_2, CH_4, and CO in the first channel equipped with a 10 m molecular sieve 5 A column; CO_2, C_2H_2, C_2H_4, and C_2H_6 in the second channel installed with a 10 m PPU column; and C_3–C_6 and $C_3^=$–$C_5^=$ ("=" denotes alkenes) in the third and fourth channels charged with a 10 m alumina column and one 8 m CP-Sil 5CB column, respectively. Ar and He were the carrier gases for the first and the remaining three channels, respectively. The composition of the gas products was used to calculate the moles of each species assuming the ideal gas law.

Based on the formed aromatic products, the defined substitution index is calculated by the equation shown below:

$$\textit{Subsitutition index of aromatic components} = \frac{\textit{Number of substituted groups}}{\textit{Number of total available substitution points}} \times \textit{molar percent}\% \times 100 \quad (1)$$

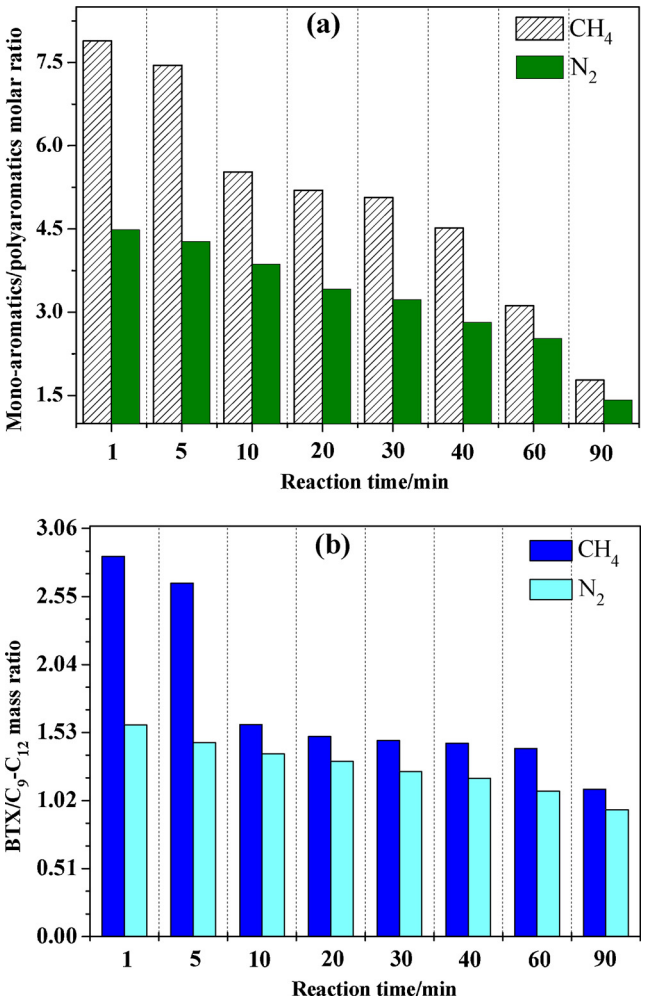

Fig. 1. The mono-aromatics/polyaromatics molar ratio (a) and BTX/C_9-C_{12} mass ratio (b) of liquid products derived from heptane conversion under CH_4 and N_2 conditions at various reaction times.

3. Results and discussions

3.1. Catalytic performance evaluation

The aromatization performance of heptane was evaluated under CH_4 and N_2 conditions at various reaction times. The heptane conversion obtained under different reaction conditions is illustrated in Fig. S1 in the Supporting information. The gaseous compositions derived from aromatization reaction at different times are shown in Table S1 in the Supporting information. According to the GC–MS analysis, the liquid products derived from heptane aromatization under different conditions were mainly BTX, and some other heavy aromatics. As shown in Fig. 1a, at the initial stage mono-aromatics are the primary products. However, further increase in reaction time leads to a significant decrease in content of light aromatics, which might be due to the occurrence of condensation for these mono-aromatic components. The ZSM-5 supported catalyst could highly promote the dehydrogenation, cyclization and aromatization of hydrocarbons [28,29], and the increased reaction time could boost the interaction between intermediate molecules and catalyst, therefore a longer reaction time leads to a lower ratio between mono- and poly-aromatics among the liquid products. To

conclude, the condensation reaction prevails when the reaction proceeds for a longer time wherein simple mono-aromatic molecules are converted to more complicated ones, leading to the increased content of poly-aromatic compounds [30].

Products prepared under both N_2 and CH_4 show similar trends, with the mono-aromatics/poly-aromatics ratio decreasing with reaction time, but the ratio is much lower when prepared under N_2 than when derived from a methane condition. Such occurrences are ascribed to two possible causes. On the one hand, methane is activated with the assistance of the charged catalyst, and then the formed CH_{4-x} moieties from methane cleavage may be incorporated into the single aromatics, resulting in the growth of smaller aromatic compounds. On the other hand, the introduced methane in the reaction system could act as a hydrogen donor. The activated hydrogen radicals would stabilize the fragments, and thus inhibit the occurrence of undesired reactions [31,32].

BTX/C_9-C_{12} mass ratios of the liquid products acquired at various times are illustrated in Fig. 1b. The ratio declines with reaction time no matter what the reaction environment is. C_9–C_{12} aromatics were composed of various types of alkylbenzene and a certain amount of naphthalene and its derivatives. The obvious decrease in BTX/C_9-C_{12} ratios might be closely associated with BTX transformation into large substituted aromatics. With the increased reaction time, the shift of chemical constituents towards a larger carbon number becomes more significant, suggesting that a longer reaction time may enhance the formation of larger aromatic components. Kim et al. [33] demonstrated a reaction pathway of hydrocarbon aromatization that involved BTX components transformation into C_9 aromatics, which were considered as the intermediates of C_{10}–C_{12} species.

Compared with a methane environment, the ratio between BTX and C_9–C_{12} was smaller when prepared under N_2 conditions, perhaps due to the methane engagement into these product molecules. The intermediates from methane conversion would participate in the formation of light aromatics. In addition, the produced hydrogen radicals provide a reduction environment that may prevent further condensation, resulting in the decreased amount of larger aromatics.

To further investigate the methane participation in the aromatic formation, the substitution degree and average carbon number derived from the aromatic composition are discussed. It is noted that the substitution index and average carbon number increase with prolonged time, indicating that the methane influence is highly enhanced. As displayed in Fig. 2a, the improved substitution index might be attributed to more methane molecules attached to phenyl rings, and thus the produced smaller aromatic compounds would be transferred into more substituted ones. Based on the decreased ratios between single aromatics and polyaromatics, it can be speculated that aromatic compounds with a certain amount of alkyl substituted groups convert into polyaromatics through cyclization and dehydrogenation. In addition, these activated alkyl species derived from methane cleavage are prone to interact with small compounds, resulting in decreased BTX fractions. In comparison with preparations under a N_2 environment, the larger substitution index obtained from methane conditions is also indicative of methane incorporation into product molecules.

As seen in Fig. 2b, the liquid product selectivity is shifted towards larger components with prolonged time. Such a phenomenon might be ascribed to the interaction between methane and formed aromatic molecules. The activated methane molecules could act as the alkyl group donor, which directly bond with the phenyl rings [34]. The increased time highly boosted the methane influence on the liquid product distribution, resulting in the increment of large product molecules. He et al. also found that the average carbon number became larger during the co-aromatization of hydrocarbons and methane [20]. The average carbon number obtained from a N_2 atmosphere was lower than that under methane conditions, which supports the viewpoint that methane was involved into the formation of product molecules. Additionally, in the case of the N_2 run, the increased average carbon

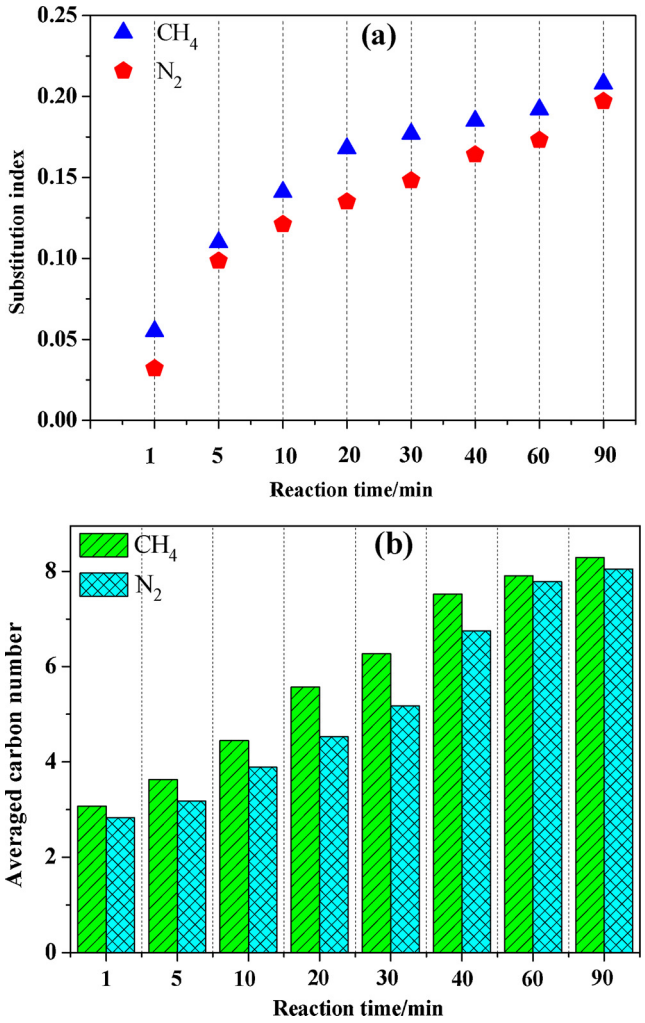

Fig. 2. The substitution index (a) and the average carbon number (b) of liquid products obtained from heptane conversion under CH_4 and N_2 condition at various reaction times.

number might be attributed to the condensation of small aromatic components with increased time, and thus a large number of heavy aromatics among the liquid products would also result in the increase of the average carbon number.

3.2. Methane engagement evidence

To strengthen the point that methane participation into the aromatization reaction, $^{13}CH_4$ was selected as the reactive atmosphere for heptane aromatization so that direct evidence related to the effect of methane on the product distribution might be observed through ^{13}C NMR analysis. Additionally, the reaction performance observed from the non-labeled methane resource was employed for a better comparison. The ^{13}C NMR spectra of liquid products collected under different conditions are illustrated in Fig. S2 in the Supporting information. To observe the difference in these spectra clearly, expanded views at two chemical shifts regions of 120–140 ppm and 10–40 ppm are displayed in Fig. S3 in the Supporting information.

Table 1 summarizes an apparent increase in peak intensity located at specific NMR sites. The signals appearing at 129.04, 128.30 and 125.41 ppm belong to ortho, meta and para position of alkyl groups in phenyl ring [35], and their lower increased degree indicate that this type of carbon site is not favorable for methane involvement at short reaction times. Thus, it can be deduced that these aromatic compounds were mainly formed from neat feedstock conversion. In addition, the

Table 1
^{13}C liquid NMR comparative peak area ratios with reference to $CDCl_3$ of products obtained from heptane aromatization under CH_4 and $^{13}CH_4$ environments at 1 min.

Chemical shift (ppm)	Peak assigned	$^{13}CH_4$	CH_4	Increase/%
129.04	Ortho positions of the alkyl substituted phenyl ring	0.07	0.06	16.07
125.41	Para positions of the alkyl substituted phenyl ring	0.05	0.04	11.36
32.20	3-C in heptane and alkyl group attach to aromatics	0.29	0.21	38.10
30.42	Benzylic carbon	0.06	0.05	14.29
29.49	4-C in heptane	0.11	0.09	17.02
23.28	2-C in heptane and alkyl group attach to aromatics	0.28	0.22	27.27
14.56	1-C in heptane	0.23	0.20	15.00

characteristic shifts of alkyl carbons are also included in the summary. The higher peak intensity of the raw feedstock is due to its poor conversion at 1 min. The peaks at 29.49 and 14.56 ppm are ascribed to the different carbon sites of heptane. However, in the case of the chemical shifts at 32.20 and 23.28 ppm, it is noted that these peaks exhibited a noticeable growth that might be attributed to two major parts. On the one hand, some types of carbon on heptane are located in these regions. On the other hand, the carbon sites of alkyl substituents attached to the phenyl ring are also present in the same region. Besides, increased intensity in benzylic carbon sites is also indicative of methane engagement into alkyl groups in aromatics. Based on these observations, it can be speculated that methane might be transferred into the substituent groups rather than aromatic rings at shorter reaction times. These results were consistent with the investigation on the co-aromatization of propane and methane [22], which suggested a possible reaction pathway that methane participation probably occurred through the interaction with aromatic molecules formed from feedstock.

To better understand the effect of methane on the aromatization process, the differences in peak intensity obtained at 30 min are listed in Table 2. When unlabeled methane was replaced by methane enriched with ^{13}C, a new signal appeared at 137.45 ppm, which was assigned to the phenyl carbon directly bonded to alkyl groups. A considerable enrichment in this peak intensity indicates that the labeled carbon atom converts into aromatic carbon with prolonged time. Additionally, a second peak at 125.86 ppm belonging to the carbon site in naphthalene and its derivatives is freshly observed. Such phenomena suggest that longer reaction times could lead to the formation of polyaromatics through further cyclization and dehydrogenation. Based on different positions of carbon sites in the phenyl ring, the peak intensity of a meta carbon site illustrated a noticeable increase, suggesting that carbon

Table 2
^{13}C liquid NMR comparative peak area ratios with reference to $CDCl_3$ of products obtained from heptane aromatization under CH_4 and $^{13}CH_4$ environments at 30 min.

Chemical shift (ppm)	Peak assigned	$^{13}CH_4$	CH_4	Increase/%
137.45	Phenyl carbon directly attached to alkyl group	0.03	0.02	32.00
129.03	Ortho positions of the alkyl substituted phenyl ring	0.13	0.11	18.18
128.30	Meta positions of the alkyl substituted phenyl ring	0.39	0.27	44.44
125.41 126.14	Para positions of the alkyl substituted phenyl ring	0.12	0.10	20.00
30.42 21.71	Benzylic carbon	0.12	0.09	27.66
29.49	4-C in heptane	0.04	0.03	14.71
14.56	1-C in heptane	0.08	0.07	19.70

Table 3
^{13}C liquid NMR comparative peak area ratios with reference to $CDCl_3$ of products obtained from heptane aromatization under CH_4 and $^{13}CH_4$ environments at 90 min.

Chemical shift (ppm)	Peak assigned	$^{13}CH_4$	CH_4	Increase/%
137.45	Phenyl carbon directly attached to alkyl group	0.04	0.02	111.76
129.04	Ortho positions of the alkyl substituted phenyl ring	0.39	0.24	62.50
128.30	Meta positions of the alkyl substituted phenyl ring	0.42	0.31	35.48
127.95 125.86	C in naphthalene ring	0.07	0.05	42.55
125.41 126.14	Para positions of the alkyl substituted phenyl ring	0.14	0.11	27.27
30.42 21.71	Benzylic carbon	0.13	0.11	18.18

atoms from methane would favor involvement in this position. As previously mentioned, methane prefers to incorporate into substitution groups attached to aromatic rings at 1 min. With prolonged time the formed CH_x moieties from methane activation might transfer into the phenyl ring, resulting in the increase on the corresponding peak intensity. The carbon sites at 30.42 and 21.71 ppm are assigned to the methyl group directly bonded to the aromatic ring, and the prominent improvement on peak intensity is attributed to the enhanced interaction between methane and reactive intermediates at longer reaction times, promoting the formation of methyl substituted aromatic components. Compared with the feedstock carbon site observed at 1 min, the greatly reduced peak intensity belonging to heptane is indicative of an enhanced conversion with prolonged time.

Based on the comparison of peak intensities at 90 min (Table 3), a significant increment of signal at 137.45 ppm, which belongs to the phenyl carbon directly bonded to alkyl groups, is observed. Thus, the increase in reaction time might lead to the transformation of ^{13}C-labeled carbon atoms into aromatic rings. In addition, there is a remarkable increase in the peak intensity at 127.95 ppm corresponding to carbon sites in polyaromatics. These observations could be attributed to the intensive reaction between active methane molecules and intermediates, which was responsible for the methane-^{13}C carbon atoms involvement into aromatic rings. The increased intensity appearing at the ortho and meta carbon sites of the phenyl rings further supports this hypothesis. Undoubtedly, the extended reaction time promotes the embedding of ^{13}C-carbon atoms into the aromatic ring due to the enhanced methane effect on the product formation. In comparison with the spectra acquired at 30 min, further increase in residence time could result in the transformation of methyl groups into phenyl rings. On the basis of this observation, it can be deduced that the ^{13}C-enrichment carbon sites in aromatic rings might be attributed to the transformation of initially formed alkyl groups into their subsequent phenyl rings, and the methane participation into aromatic compounds would be enhanced with prolonged time.

To make a comprehensive analysis on ^{13}C NMR spectra of liquid products obtained from different times, as illustrated in Fig. S4 in the Supporting information, the area ratio of dominant peaks with $CDCl_3$ employed as the internal reference are summarized in Table 4. In the case of regions belonging to aromatic products, the area ratios of carbon sites in substituted phenyl rings are illustrated in Fig. 3a. As the reaction time increases from 1 to 30 min, the peak area ratio in terms of meta carbon sites showed a substantial increase in comparison with that of other carbon positions. This result might be attributed to the transfer of alkyl substituent groups in phenyl rings with prolonged time. However, further increase in reaction time may promote methane incorporation into the ortho carbon sites. On the one hand, the meta position of substituted aromatics might transform into ortho position

Table 4
^{13}C liquid NMR comparative peak area ratios with reference to $CDCl_3$ of products obtained from heptane aromatization under $^{13}CH_4$ environment at different reaction time.

Chemical shift (ppm)	Peak assigned	1 min	30 min	90 min
137.45	Phenyl carbon directly attached to alkyl group	–	0.03	0.04
129.04	Ortho positions of the alkyl substituted phenyl ring	0.07	0.13	0.39
128.30	Meta positions of the alkyl substituted phenyl ring	0.07	0.39	0.42
127.95	C in naphthalene ring	–	0.04	0.07
125.86				
125.41	Para positions of the alkyl substituted phenyl ring	0.049	0.12	0.14
126.14				
32.28	3-C in heptane	0.29	0.05	0.03
30.42	Benzylic carbon	0.056	0.12	0.13
21.71				
23.28	2-C in heptane	0.28	0.05	0.02
14.56	1-C in heptane	0.23	0.08	0.02

through a rearrangement reaction [36], but the alkyl group from methane cleavage would interact with aromatic compounds, resulting in the increased ortho carbon sites.

In addition, the peak intensity of carbon sites assigned to polyaromatics increased with extended time, which is consistent with previous observations on the decreased BTX/ C_9–C_{12} ratio. The increased area of alkyl group peaks at 30.42 and 21.71 ppm (Fig. 3b) is in agreement with the aforementioned increased substitution index, suggesting that prolonged time might boost the interaction between the activated methane species and intermediates derived from heptane conversion. In terms of peak shifts assigned to the raw feedstock, it is clearly observed that the characteristic peak ratio from heptane gradually reduced due to the enhanced conversion with prolonged time. Based on the product distributions, these carbon atoms in feedstocks could be converted into the aromatic compounds, and then react with activated methane to form the substituted aromatic derivatives. Besides, the peaks belonging to alkyl carbon sites indirectly attached to the phenyl rings were not found in the spectra, implying that methane prefers to participate into the benzylic carbon sites rather than other alkyl positions.

Fig. 4 depicts qualitative ^{13}C CP/MAS NMR spectra of the adsorbed reaction intermediates on the catalyst surface formed from heptane aromatization under CH_4 and $^{13}CH_4$ conditions at various times. In the case of the reaction after 1 min, strong ^{13}C NMR signals at 30.1, 22.7, and 13.3 ppm appear in the spectra, which belong to the raw feedstock. In addition, the signal at 127.8 ppm is attributed to the carbon site of substituted aromatic compounds, and the peak at 18.6 ppm is due to the methyl groups attached to phenyl rings formed in the reaction [37,38]. The weak signal at 137.1 ppm is assigned to the phenyl carbon directly bonded to alkyl groups. It is worth noting that the weak intensity of this peak does not necessarily indicate that the concentration of this carbon is low. It might be due to the lack of surrounding H atoms, which are required to enhance the ^{13}C NMR signal in CP/MAS NMR spectra. In comparison with the spectrum acquired under unlabeled CH_4 conditions, the signal at 18.6 ppm increased notably, suggesting that initially the carbon atom of activated methane species convert into the methyl group attached to phenyl rings. With respect to reactions occurred at 30 and 90 min (Fig. 4b and c), the signals appearing at 127.8 and 18.6 ppm exhibit an enhancement when the unlabeled CH_4 was replaced with methane enriched with ^{13}C. Thus, such results indicate that the methane is involved in the aromatization process, and that the phenyl and alkyl carbon sites are favorable to methane engagement with prolonged time. In addition, based on the notable enhancement of these signals, it can be concluded that methane is highly activated on the catalyst surface and then incorporated during the aromatic formation process. Compared with the case at 1 min, the increased reaction times result in noticeable enrichment in peak intensities at 127.8 and 137.1 ppm, suggesting that the ^{13}C atoms from methane can convert into the carbon sites of substituted aromatics.

Simultaneously, the intensity of the peak at 18.6 ppm observed at 30 min under a ^{13}C-labeled methane environment showed no obvious change in comparison with that at 90 min. This might be attributed to the ^{13}C-labeled carbon atom of alkyl group transformation into phenyl rings, which is consistent with the observation in liquid NMR results discussed above. As the reaction proceeds, the prolonged time also leads to the decrease of peak intensity belonging to heptane, owing to the enhanced conversion.

3.3. Reaction mechanism

According to the ^{13}C NMR differences observed with increased time, two possible reaction pathways on the labeled ^{13}C atom of methyl group transformation into phenyl ring are hypothesized, as illustrated in Figs. 5 and 6. As mentioned in previous literature, it is proposed that the methane-to-aromatic reaction proceeds based on the methylation of aromatic molecules, which are initially formed from raw feedstock conversion on Zn- and Ga-modified zeolites [22]. Initially, the methane activation is triggered by the engaged catalyst, and thus alkyl group intermediates derived from methane cracking would interact with the aromatic compound derived from heptane conversion to form methyl substituted phenyl rings. The phenylmethyl cation is produced through dehydrogenation with the assistance of a metal-loaded zeolite catalyst,

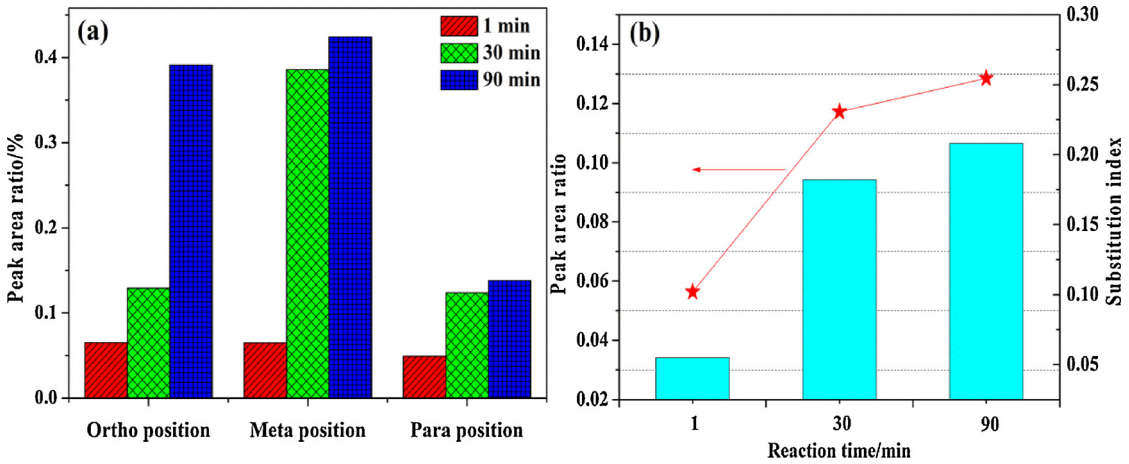

Fig. 3. The peak area ratio of substituted phenyl rings (a) and the peak area ratio of benzylic carbon site correlated with their corresponding substitution index (b) acquired from heptane conversion under $^{13}CH_4$ condition at various reaction times.

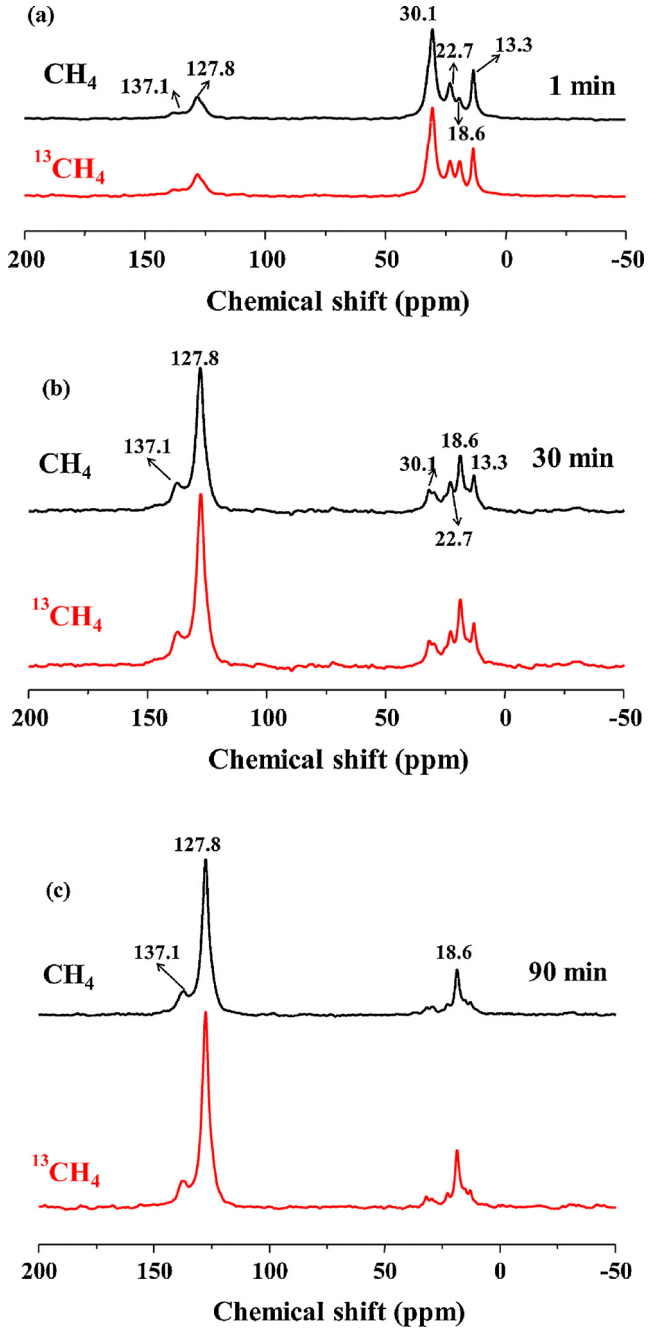

Fig. 4. ^{13}C CP/MAS NMR spectra of the products derived from heptane conversion under $^{13}CH_4$ and CH_4 conditions at 1 min (a), 30 min (b) and 90 min (c).

and then three-member rings are expected to be formed via an electrophilic pathway [39]. Moreover, through a ring expansion/contraction mechanism the CH_x moieties formed from methane activation could engage into aromatic carbon sites [24]. As shown in Fig. 5a, the labeled carbon-13 atom might be incorporated into the varied substituted sites of phenyl rings. The other possible approach referred to the methane-^{13}C transformation into the phenyl carbon sites directly bonded to the alkyl group is shown in Fig. 5b, which is in agreement with the enhanced aromatic peak intensities with increased time.

It should be noted that naphthalene and its derivatives were formed with increased time, which might be due to the cyclization and dehydrogenation of methyl-substituted aromatics over the metal-modified ZSM-5 acidic support [40]. Thus, the ^{13}C atom of the methyl group may convert into the carbon sites in the polyaromatic species (Fig. 6) at longer times, resulting in enhanced signals due to naphthalene carbon sites.

3.4. Catalyst characterizations

To gain a comprehensive understanding of the correlation between the physical properties of Zn-Ga/ZSM-5 catalysts and their corresponding catalytic performance, versatile characterization techniques including XAS, XPS, TEM, and NH_3-TPD have been engaged in this study.

XAS is one of the most powerful techniques that can be used to investigate the oxidation state and local environment of metal species loaded on the zeolite support. It is worth nothing that the signals arising from gallium species are not observed in these tested samples, which is possibly due to its significantly lower concentration on the catalyst. Thus, the chemical environment of Zn species is mainly discussed here through the analysis of the obtained XAS spectra.

The Zn L-edge spectra of ZnO, $Zn(NO_3)_2$, fresh Zn-Ga/ZSM-5, and spent catalysts obtained from different reaction atmospheres are illustrated in Fig. 7. Generally, TFY signals are collected from the bulk of particles whereas the TEY are attributed to the metal species distributed on the external surface of solid samples. The adsorption threshold (E_0) at around 1028 eV observed from these catalysts is related to the Zn 3d-derived state, which is different from featured peaks of pure ZnO and $Zn(NO_3)_2$ samples [41]. Such results suggest that the local environment of Zn species on these catalysts might be affected by the zeolite support. When compared with the pure ZnO sample, the increase of peak intensity may be due to an enhancement of O 2p-Zn 3d anti-bonding coupling [42], which was derived from the interaction between Zn species and O atoms in the zeolite framework.

XPS analysis was carried out on Zn and Ga modified ZSM-5 catalyst to get more information about the chemical state of metal species. As exhibited in Fig. 8a, Zn $2p_{1/2}$ and Zn $2p_{3/2}$ signals achieved from various samples are observed at a binding energy of 1046.22 and 1023.06 eV, which illustrates a slight difference from the ZnO species existing on the surface of the catalyst. This observation is consistent with the XAS results that indicate that the interaction between Zn and O from the zeolite framework results in a changed chemical environment of the Zn species [43,44]. In the case of spent catalysts collected under methane conditions, there is a slightly decreased intensity of Zn peaks detected in the spectra. Thus, it is speculated that Zn species might migrate into the inner pore of the zeolite support, and the introduced methane would be favorable to the dispersion of metal species on the catalyst surface. On the contrary, the enhanced peak intensity observed from a N_2 atmosphere may be attributed to the agglomeration of loaded metal, resulting in a poorer distribution.

As can be seen in Fig. 8b, the binding energy at 1118.86 eV is ascribed to the Ga $2p_{3/2}$ band, which demonstrates that the nature of the loaded Ga species is close to that of Ga_2O_3 with the highest oxidation state [45,46]. No significant changes are observed for these two spectra acquired from CH_4 and N_2 conditions, suggesting that the Ga valence state is relatively stable. Compared with the fresh sample, the similar peak intensity implies that the gallium species are mostly maintained on the surface of catalyst during the aromatization reaction. Based on the above observation, the Ga species with stable dispersion and highest oxidation state might be responsible for the excellent aromatization ability.

With regards to the C peaks on the fresh sample (Fig. 8c), the minor carbon signal at 284.80 eV belongs to the adsorbed CO_2 or some carbon-containing compounds attached on the surface. The highly increased peak intensity from spent catalysts is indicative of coke formation during the reaction process. As expected, relatively lower carbon peak intensity was obtained from the methane run in comparison with its N_2 counterpart. It can be concluded that the provided hydrogen radicals from methane cracking might facilitate inhibiting further condensation of large components, thus resulting in reduced

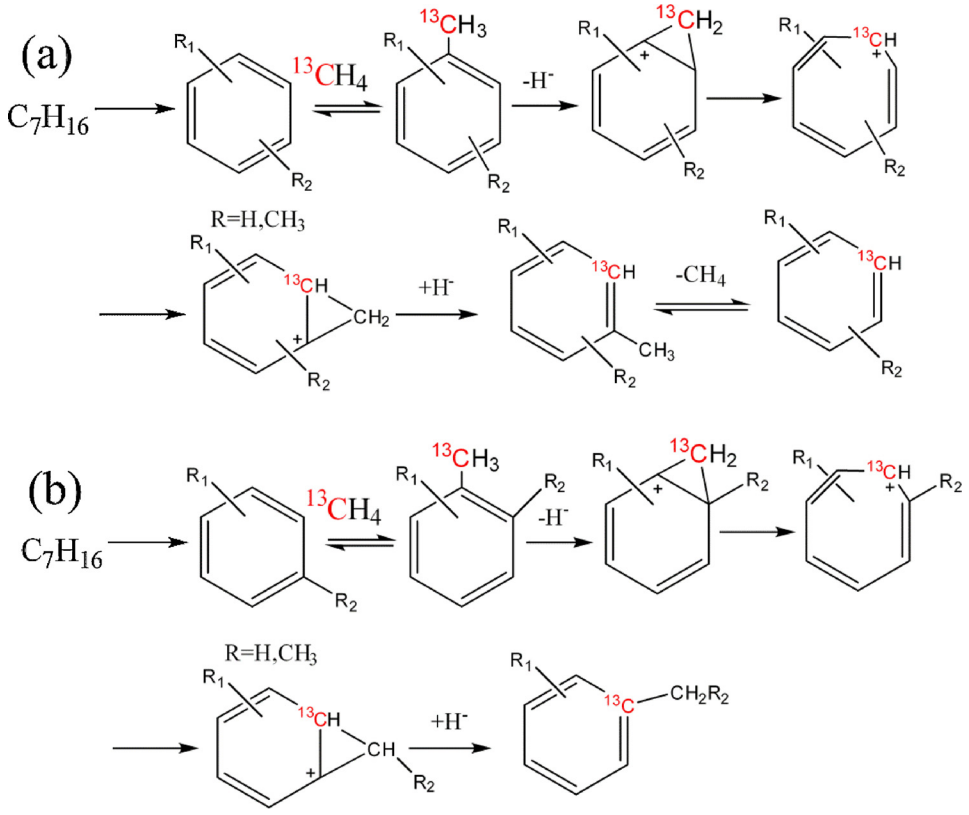

Fig. 5. Possible reaction pathways of labeled ^{13}C from methyl group into the aromatic carbon atom in phenyl ring formed from $^{13}CH_4$ and heptane co-aromatization.

coke formation under a methane environment. Such observations are consistent with the liquid production distribution under CH_4 and N_2 conditions. A large quantity of polyaromatic components produced from the N_2 run are the precursors of coke formed on the catalyst surface, and thus the observed carbon peak intensity is stronger than that from the methane environment.

The spectra at O 1s region are illustrated in Fig. 8d. Only one O signal was detected in these samples. The binding energy at 532.89 eV may be attributed to the SiOH group that exists in the framework of the zeolite with high abundance [47]. However, the oxygen species contributed by the metal oxides were hardly detected from the spectra, perhaps because of the much lower concentration on the surface of catalyst. Furthermore, the migration of some metal oxide compounds into the inner structure also supports the reduced oxygen surface concentration.

The TEM characterization with EELS was employed to study the morphology and particle size as well as the metal dispersion of the engaged catalyst. As illustrated in Fig. 9a and b, the images of fresh catalysts obtained with two magnifications indicate that loaded metal particles are dispersed well on the whole surface of the zeolite support. In the case of the spent catalyst collected from the methane run, the image in Fig. 9c shows that much smaller particles are observed after a thorough morphology scan, suggesting that the presence of methane might promote the high dispersion of metal species and thus play a positive role on the feedstock and methane conversion. However, as displayed in Fig. 9d, the particle size obtained under a N_2 environment increased compared to the fresh one, implying the occurrence of particle agglomeration under inert gas conditions.

Furthermore, the metal species distribution on the surface of the catalyst was investigated by using the EELS technique. As shown in Fig. 10, the exhibited bright spots are proportional to the amount of loaded Zn and Ga encountered by the electron beam in the specific area, which afford detailed information related to the metal distribution. The Zn and Ga maps for fresh and spent samples under different reaction atmospheres were obtained by using the Zn-M and Ga-L peaks, respectively. Compared with the fresh sample in Fig. 10a, as shown in Fig. 10c, the light spots distributed on the border collected from the N_2 run exhibit a higher density, suggesting that accumulation of Zn particles occurs to a certain extent whereas this phenomenon is not found under the methane condition. Therefore, it is further confirmed that the introduced methane is beneficial for metal dispersion during the reaction process. Nevertheless, as to Ga distribution in Fig. 10d–f, the insignificant change of Ga dispersion obtained from CH_4 and N_2 conditions indicate that the Ga species are maintained on the catalyst surface well after the reaction. Such observations are consistent with the Ga distribution witnessed from XPS spectra.

To further investigate the reactive environment effect on the structural features of these catalysts, the surface acidic sites were analyzed by using NH_3-TPD, the profiles of which are exhibited in Fig. 11. Additionally, the detailed information related to the quantification of distributed acidic peaks is summarized in Table 5. In the case of pure ZSM-5, the desorption peak distributed in the low temperature region

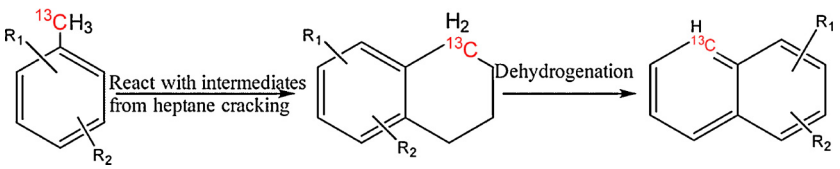

Fig. 6. Possible reaction pathway (a and b) of labeled ^{13}C from methyl group into the aromatic carbon atom in phenyl ring formed from $^{13}CH_4$ and heptane co-aromatization.

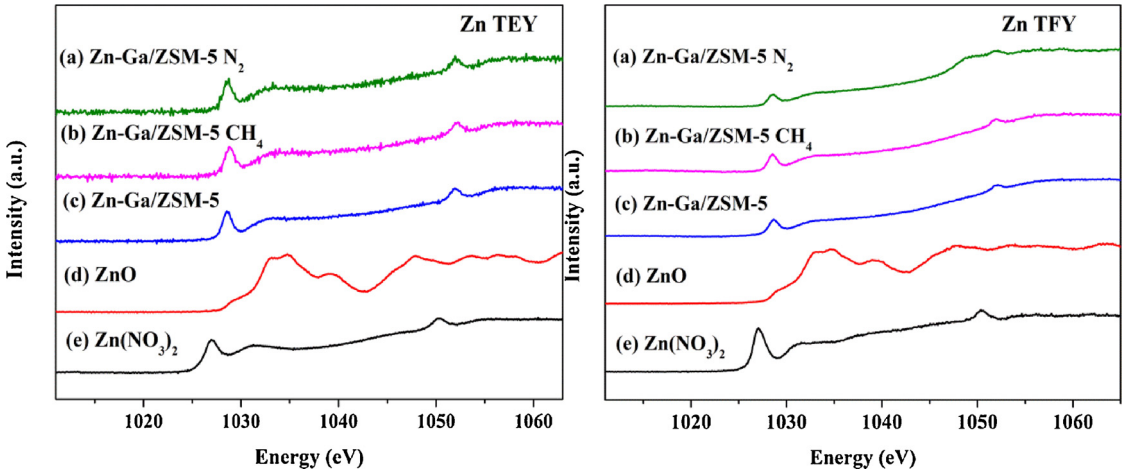

Fig. 7. Zn L-edge XANES spectra including TEY and TFY signals of $Zn(NO_3)_2$, ZnO fresh Zn-Ga/ZSM-5 and spent samples collected from CH_4 and N_2 environments.

spanning from 200 to 400 °C is assigned to the weak acidic sites whereas the other obvious peak located at the high temperature region ranging from 400 to 600 °C is referred to as strong surface acidic sites [48,49]. However, compared with that from the conventional zeolite, the intensity of the high temperature peak upon metal modification is reduced significantly, which may be ascribed to the occupation of introduced Zn and Ga species on the original acidic sites. As to these metal-modified samples, the presence of strong acidic sites with smaller amounts suggest the availability of strong Brönsted and Lewis acid sites [50]. Interestingly, a newly formed peak centered at around 300 °C was observed from metal loaded catalysts after NH_3 treatment, which is defined as the medium acidic site. According to previous research, the highly dispersed metal species on the catalyst surface could interact with acidic protons from the zeolite framework to generate the new acidic sites [31]. As displayed in Table 5, it is worth noting that the relative amounts of weak and medium acidity account for a large

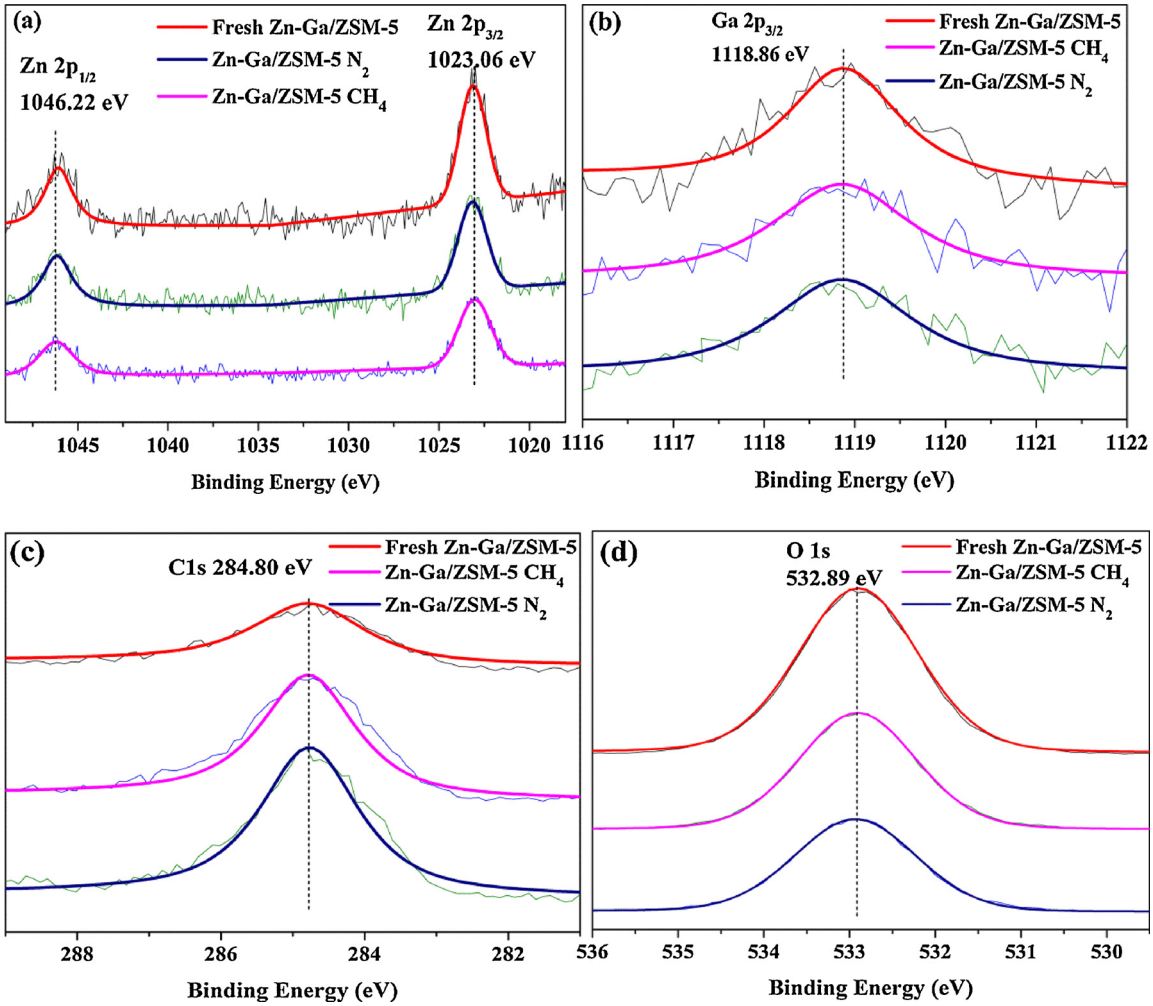

Fig. 8. Zn 2p (a), Ga $2p_{3/2}$ (b), C 1s (c) and O 1s (d) XPS spectra of Zn-Ga/ZSM-5 before and after heptane reaction under CH_4 and N_2 environments.

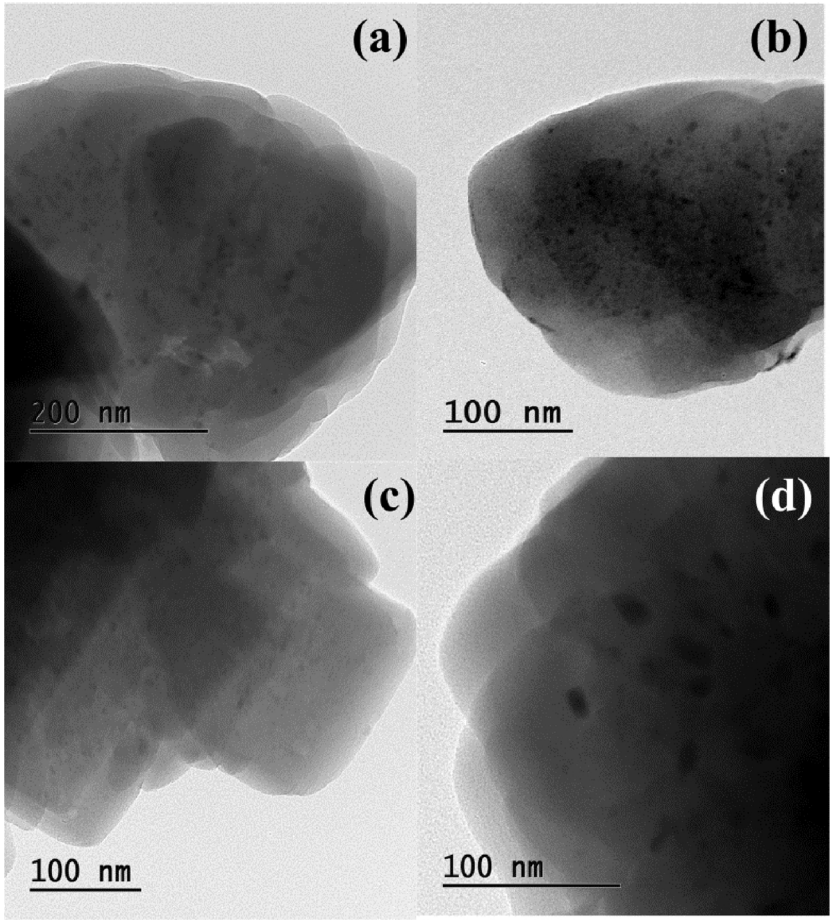

Fig. 9. TEM images of fresh Zn-Ga/ZSM-5 (a and b) and spent samples obtained under CH_4 (c) and N_2 (d) atmospheres.

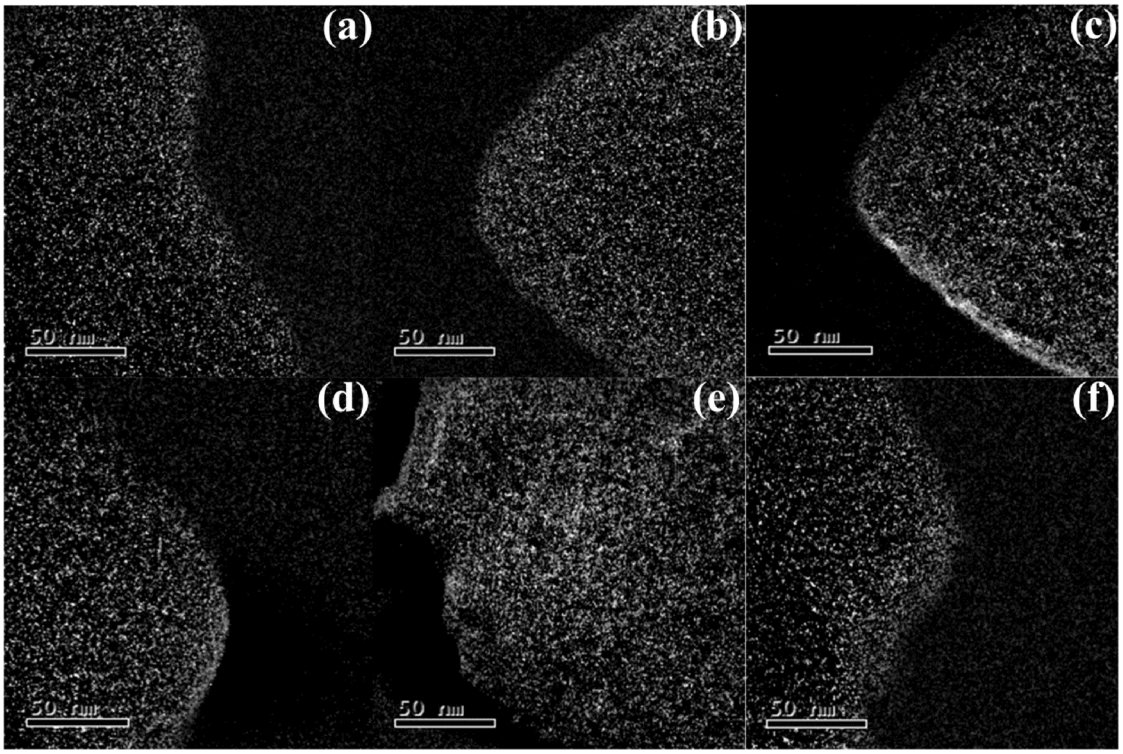

Fig. 10. EELS images of Zn-M in terms of fresh Zn-Ga/ZSM-5 (a), and spent samples collected under CH_4 (b) and N_2 (c) conditions; EELS images of Ga-L in terms of fresh Zn-Ga/ZSM-5 (d), and spent samples collected under CH_4 (e) and N_2 (f) conditions.

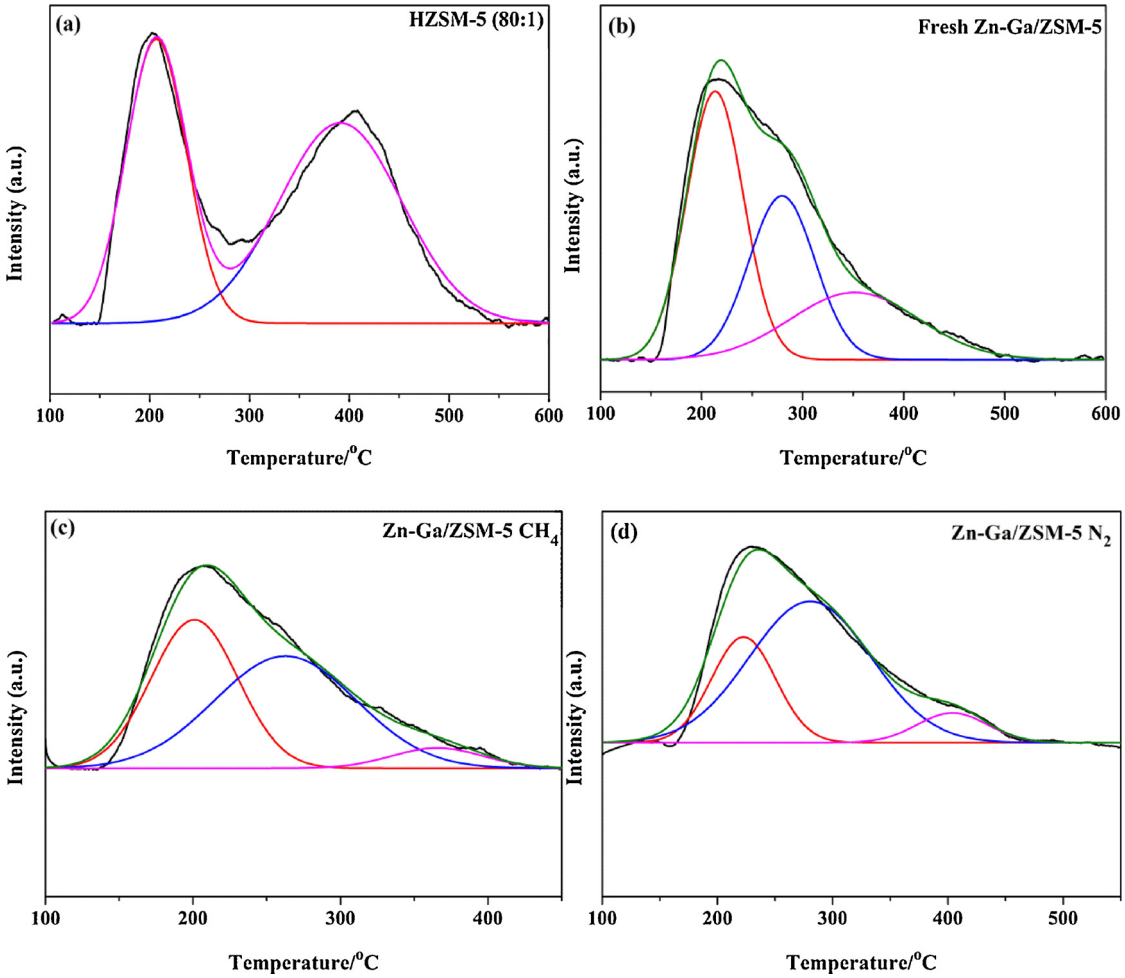

Fig. 11. NH_3-TPD profiles of ZSM-5 (a), fresh (b) and spent Zn-Ga/ZSM-5 (c and d) collected under different reaction atmospheres.

Table 5
Summary of surface acidity distribution from different samples.

Catalyst	Total acidity (μmol NH_3/g cat)	Weak	Medium	Strong
HZSM-5	1047	430	0	617
Fresh Zn-Ga/ZSM-5	939	414	292	232
Zn-Ga/ZSM-5 CH_4	571	241	296	34
Zn-Ga/ZSM-5 N_2	207	54	137	16

proportion of all surface acidity on the fresh catalyst. Such observations indicate that the existing weak and medium acid sites play a vital role on the excellent catalytic performance.

After the reaction, the total acid amount of the spent catalyst showed a dramatic reduction in comparison with that of its original one. Moreover, the acidity amount from the N_2 run decreased to a large extent, indicating that more coke was deposited on the surface acidic sites after the aromatization reaction, which is consistent with carbon distribution observed in the XPS results. The coke suppression in terms of the methane condition could be related to the reduction environment provided by reactive methane as a hydrogen donor. Thus, the relatively large quantity of acidity still remaining on the sample might be responsible for the improved upgrading performance on the feedstock conversion under methane conditions.

4. Conclusions

The present research demonstrates the co-aromatization of methane and heptane upon Zn-Ga modified catalyst at various times. The H_x and CH_x intermediates derived from methane activation would incorporate into the formed light aromatics, and highly suppress further condensation, resulting in a decreased amount of heavy aromatics in comparison with its N_2 counterpart. In addition, the increased average carbon number and substitution index of liquid products are indicative of methane participation into aromatization processes. Application of ^{13}C NMR spectroscopy on the analysis of the joint conversion between methane and heptane showed that the methane might favor participation into phenyl carbon and benzylic carbon sites with increased time. The excellent behavior of Zn-Ga/ZSM-5 may be related to the high dispersion of metal species and a certain amount of medium and weak acidic sites. The introduced methane is responsible for the coke suppression and metal agglomeration prohibition, and thus plays a positive role on the feedstock conversion.

Acknowledgements

We gratefully acknowledge the financial supports from Shandong Chambroad Petrochemicals Co., Ltd and Natural Sciences and Engineering Research Council of Canada (NSERC). We also appreciate the XAS facilities provided by the Canadian Light Source.

Appendix A. Supplementary data

Supplementary material related to this article can be found, in the online version, at doi:https://doi.org/10.1016/j.apcatb.2018.05.006.

References

[1] Z. Cao, H. Jiang, H. Luo, S. Baumann, W.A. Meulenberg, J. Assmann, L. Mleczko, Y. Liu, J. Caro, Natural gas to fuels and chemicals: improved methane aromatization in an oxygen-permeable membrane reactor, Angew. Chem. Int. Ed. Engl. 52 (2013) 13794–13797.

[2] V. Abdelsayed, D. Shekhawat, M.W. Smith, Effect of Fe and Zn promoters on Mo/HZSM-5 catalyst for methane dehydroaromatization, Fuel 139 (2015) 401–410.

[3] J.J. Spivey, G. Hutchings, Catalytic aromatization of methane, Chem. Soc. Rev. 43 (2014) 792–803.

[4] J. Xu, A. Zheng, X. Wang, G. Qi, J. Su, J. Du, Z. Gan, J. Wu, W. Wang, F. Deng, Room temperature activation of methane over Zn modified H-ZSM-5 zeolites: insight from solid-state NMR and theoretical calculations, Chem. Sci. 3 (2012) 2932.

[5] P. Schwach, X. Pan, X. Bao, Direct conversion of methane to value-added chemicals over heterogeneous catalysts: challenges and prospects, Chem. Rev. 117 (2017) 8497–8520.

[6] R.H. Crabtree, Aspects of methane chemistry, Chem. Rev. 95 (1995) 987–1007.

[7] P. Tang, Q. Zhu, Z. Wu, D. Ma, Methane activation: the past and future, Energy Environ. Sci. 7 (2014) 2580–2591.

[8] X. Guo, G. Fang, G. Li, H. Ma, H. Fan, L. Yu, C. Ma, X. Wu, D. Deng, M. Wei, Direct, nonoxidative conversion of methane to ethylene, aromatics, and hydrogen, Science 344 (2014) 616–619.

[9] J.H. Lunsford, The catalytic oxidative coupling of methane, Angew. Chem. Int. Ed. 34 (1995) 970–980.

[10] L. Chen, J. Lin, H. Zeng, K. Tan, Non-oxidative methane conversion into aromatics on mechanically mixed Mo/HZSM-5 catalysts, Catal. Commun. 2 (2001) 201–206.

[11] W. Ding, S. Li, G.D. Meitzner, E. Iglesia, Methane conversion to aromatics on Mo/H-ZSM5: structure of molybdenum species in working catalysts, J. Phys. Chem. B 105 (2001) 506–513.

[12] H. Liu, S. Yang, S. Wu, F. Shang, X. Yu, C. Xu, J. Guan, Q. Kan, Synthesis of Mo/TNU-9 (TNU-9 Taejon National University No. 9) catalyst and its catalytic performance in methane non-oxidative aromatization, Energy 36 (2011) 1582–1589.

[13] V.R. Choudhary, A.K. Kinage, T.V. Choudhary, Low-temperature nonoxidative activation of methane over H-galloaluminosilicate (MFI) zeolite, Science 275 (1997) 1286–1288.

[14] M.V. Luzgin, V.A. Rogov, S.S. Arzumanov, A.V. Toktarev, A.G. Stepanov, V.N. Parmon, Understanding methane aromatization on a Zn-modified high-silica zeolite, Angew. Chem. Int. Ed. Engl. 47 (2008) 4559–4562.

[15] O.A. Anunziata, G.A. Eimer, L.B. Pierella, Catalytic conversion of natural gas with added ethane and LPG over Zn-ZSM-11, Appl. Catal. A 190 (2000) 169–176.

[16] J.F. Liu, Y. Liu, L.F. Peng, Aromatization of methane by using propane as co-reactant over cobalt and zinc-impregnated HZSM-5 catalysts, J. Mol. Catal. A Chem. 280 (2008) 7–15.

[17] O.A. Anunziata, G.V.G. Mercado, L.B. Pierella, Catalytic activation of methane using n-pentane as co-reactant over Zn/H-ZSM-11 zeolite, Catal. Lett. 87 (2003) 167–171.

[18] O.A. Anunziata, G.G. Mercado, Methane transformation using light gasoline as Co-Reactant over Zn/H-ZSM11, Catal. Lett. 107 (2006) 111–116.

[19] M.Y. Gim, C. Song, T.H. Kim, J.H. Song, D.H. Kim, K.-Y. Lee, I.K. Song, BTX production by coaromatization of methane and propane over gallium oxide supported on mesoporous HZSM-5, Mol. Catal. 439 (2017) 134–142.

[20] P. He, R. Gatip, M. Yung, H. Zeng, H. Song, Co-aromatization of olefin and methane over Ag-Ga/ZSM-5 catalyst at low temperature, Appl. Catal. B: Environ. 211 (2017) 275–288.

[21] O. Anunziata, Improvement of methane activation using n-hexane as co-reactant over Zn/HZSM-11 zeolite, Catal. Commun. 5 (2004) 401–405.

[22] M.V. Luzgin, V.A. Rogov, S.S. Arzumanov, A.V. Toktarev, A.G. Stepanov, V.N. Parmon, Methane aromatization on Zn-modified zeolite in the presence of a co-reactant higher alkane: how does it occur? Catal. Today 144 (2009) 265–272.

[23] T. Baba, Y. Abe, Metal cation–acidic proton bifunctional catalyst for methane activation: conversion of 13CH4 in the presence of ethylene over metal cations-loaded H-ZSM-5, Appl. Catal. A 250 (2003) 265–270.

[24] M.V. Luzgin, A.A. Gabrienko, V.A. Rogov, A.V. Toktarev, V.N. Parmon, A.G. Stepanov, The “Alkyl” and “Carbenium” pathways of methane activation on Ga-Modified zeolite BEA: 13C solid-state NMR and GC-MS study of methane aromatization in the presence of higher alkane, J. Phys. Chem. C 114 (2010) 21555–21561.

[25] A. Wang, D. Austin, A. Karmakar, G.M. Bernard, V.K. Michaelis, M.M. Yung, H. Zeng, H. Song, Methane upgrading of acetic acid as a model compound for a biomass-derived liquid over a modified zeolite catalyst, ACS Catal. 7 (2017) 3681–3692.

[26] A. Guo, C. Wu, P. He, Y. Luan, L. Zhao, W. Shan, W. Cheng, H. Song, Low-temperature and low-pressure non-oxidative activation of methane for upgrading heavy oil, Catal. Sci. Technol. 6 (2016) 1201–1213.

[27] P. He, Y. Luan, L. Zhao, W. Cheng, C. Wu, S. Chen, H. Song, Catalytic bitumen partial upgrading over Ag-Ga/ZSM-5 under methane environment, Fuel Process. Technol. 156 (2017) 290–297.

[28] V.R. Choudhary, D. Panjala, S. Banerjee, Aromatization of propene and n-butene over H-galloaluminosilicate (ZSM-5 type) zeolite, Appl. Catal. A 231 (2002) 243–251.

[29] N. Viswanadham, G. Muralidhar, T.S.R.P. Rao, Cracking and aromatization properties of some metal modified ZSM-5 catalysts for light alkane conversions, J. Mol. Catal. A Chem. 223 (2004) 269–274.

[30] M. Miyamoto, K. Mabuchi, J. Kamada, Y. Hirota, Y. Oumi, N. Nishiyama, S. Uemiya, Para-selectivity of silicalite-1 coated MFI type galloaluminosilicate in aromatization of light alkanes, J. Porous Mater. 22 (2015) 769–778.

[31] Y. Lou, P. He, L. Zhao, W. Cheng, H. Song, Olefin upgrading over Ir/ZSM-5 catalysts under methane environment, Appl. Catal. B: Environ. 201 (2017) 278–289.

[32] P. He, Y. Lou, H. Song, Olefin upgrading under methane environment over Ag-Ga/ZSM-5 catalyst, Fuel 182 (2016) 577–587.

[33] Y.H. Kim, K.H. Lee, J.S. Lee, The effect of pre-coking and regeneration on the activity and stability of Zn/ZSM-5 in aromatization of 2-methyl-2-butene, Catal. Today 178 (2011) 72–78.

[34] X. Wang, J. Xu, G. Qi, B. Li, C. Wang, F. Deng, Alkylation of benzene with methane over ZnZSM-5 zeolites studied with solid-state NMR spectroscopy, J. Phys. Chem. C 117 (2013) 4018–4023.

[35] E. Pretsch, P. Buehlmann, C. Affolter, E. Pretsch, P. Bhuhlmann, C. Affolter, Structure Determination of Organic Compounds, Springer, 2000.

[36] N.M. Tukur, S. Al-Khattaf, Comparison studies of xylene isomerization and disproportionation reactions between SSZ-33, TNU-9, mordenite and ZSM-5 zeolite catalysts, Chem. Eng. J. 166 (2011) 348–357.

[37] A.A. Gabrienko, S.S. Arzumanov, I.B. Moroz, A.V. Toktarev, W. Wang, A.G. Stepanov, Methane activation and transformation on Ag/H-ZSM-5 zeolite studied with solid-state NMR, J. Phys. Chem. C 117 (2013) 7690–7702.

[38] M.V. Luzgin, A.V. Toktarev, V.N. Parmon, A.G. Stepanov, Coaromatization of methane with propane on Mo-Containing zeolite H-BEA: a solid-state NMR and GC-MS study, J. Phys. Chem. C 117 (2013) 22867–22873.

[39] Y. Ono, Transformation of lower alkanes into aromatic hydrocarbons over ZSM-5 zeolites, Catal. Rev. 34 (2006) 179–226.

[40] Y. Choi, J. Lee, J. Shin, S. Lee, D. Kim, J.K. Lee, Selective hydroconversion of naphthalenes into light alkyl-aromatic hydrocarbons, Appl. Catal. A 492 (2015) 140–150.

[41] A. Sharma, M. Varshney, H.J. Shin, B.-H. Lee, K.H. Chae, S.O. Won, Effect of Cu insertion on structural, local electronic/atomic structure and photocatalyst properties of TiO2, ZnO and Ni(OH)2 nanostructures: XANES-EXAFS study, Mater. Chem. Phys. 191 (2017) 129–144.

[42] Z. Wang, L. Wu, J. Zhou, Z. Jiang, B. Shen, Chemoselectivity-induced multiple interfaces in MWCNT/Fe3O4@ZnO heterotrimers for whole X-band microwave absorption, Nanoscale 6 (2014) 12298–12302.

[43] H. Long, F. Jin, G. Xiong, X. Wang, Effect of lanthanum and phosphorus on the aromatization activity of Zn/ZSM-5 in FCC gasoline upgrading, Microporous Mesoporous Mater. 198 (2014) 29–34.

[44] A.A. Gabrienko, S.S. Arzumanov, A.V. Toktarev, I.G. Danilova, I.P. Prosvirin, V.V. Kriventsov, V.I. Zaikovskii, D. Freude, A.G. Stepanov, Different efficiency of Zn2++ and ZnO species for methane activation on Zn-modified zeolite, ACS Catal. 7 (2017) 1818–1830.

[45] H. Xiao, J. Zhang, X. Wang, Q. Zhang, H. Xie, Y. Han, Y. Tan, A highly efficient Ga/ZSM-5 catalyst prepared by formic acid impregnation and in situ treatment for propane aromatization, Catal. Sci. Technol. 5 (2015) 4081–4090.

[46] S. Tamiyakul, S. Anutamjarikun, S. Jongpatiwut, The effect of Ga and Zn over HZSM-5 on the transformation of palm fatty acid distillate (PFAD) to aromatics, Catal. Commun. 74 (2016) 49–54.

[47] K.A. Almeida, R. Landers, D. Cardoso, Properties of faujasite zeolites containing methyl-substituted ammonium cations, J. Catal. 294 (2012) 151–160.

[48] Y. Ni, A. Sun, X. Wu, G. Hai, J. Hu, T. Li, G. Li, The preparation of nano-sized H[Zn, Al]ZSM-5 zeolite and its application in the aromatization of methanol, Microporous Mesoporous Mater. 143 (2011) 435–442.

[49] J. Zhang, W. Qian, C. Kong, F. Wei, Increasing para-Xylene selectivity in making aromatics from methanol with a surface-modified Zn/P/ZSM-5 catalyst, ACS Catal. 5 (2015) 2982–2988.

[50] P. He, W. Shan, Y. Xiao, H. Song, Performance of Zn/ZSM-5 for in situ catalytic upgrading of pyrolysis bio-oil by methane, Top. Catal. 59 (2015) 86–93.